Distributed Model Predictive Control Strategy Based on Battery State and Degradation Awareness for V2G Frequency Response in Charging Stations

Song Ke, Weijie Mai, Jinpeng Tian, Ruohan Guo, Shangyang He, and Chi Yung Chung

***Abstract*—The lack of battery state and degradation awareness in electric vehicles (EVs) participating in vehicle-to-grid (V2G) frequency response (FR) can accelerate battery degradation and impair frequency support. To address this issue, we propose a distributed model predictive control (DMPC) strategy based on battery state and degradation awareness for V2G FR in charging stations (CSs), explicitly integrating battery state and degradation into the proposed strategy. First, a resistor-capacitor (RC) equivalent circuit model of batteries is integrated into the V2G FR. This allows the controller to capture internal battery states including state-of-charge and battery degradation rate. The model also monitors signals such as voltage and current, thereby enhancing both model fidelity and practical implementability. Second, an equivalent degradation model of batteries is embedded within the V2G FR, enabling the controller to jointly account for battery state and degradation while supporting V2G FR. Finally, a cross-scale hierarchical framework for V2G control strategy is developed to decouple and coordinate battery-level states and grid-level power dispatch, achieving hierarchical coordination across individual batteries and the CS. Simulation results demonstrate that the proposed DMPC strategy improves frequency regulation effectiveness, limits V2G FR tracking deviation, enhances battery operation safety and degradation preservation, and achieves more balanced V2G FR power allocation among EVs.**

***Index Terms*—Vehicle-to-grid (V2G), frequency response, distributed model predictive control (DMPC), electric vehicle (EV), charging station (CS), battery state, battery degradation.**

I. Introduction

ELECTRIC vehicles (EVs), as environmentally friendly alternatives to conventional internal combustion engine vehicles, have become a major focus in the future development of the automotive industry. Most research works about vehicle-to-grid (V2G) [1]-[3] focus on V2G at the scheduling and optimization level, coordinating EVs with storage and generation to reduce costs and demonstrate potential value of V2G. The power provided by V2G is no longer limited to peak shaving and energy balancing, but is increasingly utilized in the scenarios involving sudden load surges and grid resilience restoration [4], [5]. EVs have also emerged as a valuable resource for grid frequency support through V2G technology [6], [7].

Given the widespread use of the system frequency response (SFR) framework in modeling frequency dynamics for load frequency control (LFC) [8], V2G control often employs a similar approach, incorporating EVs as load-side controllable resources for frequency recovery analysis. The large-capacity batteries in EVs provide them with substantial potential for frequency response (FR) [9]. EVs are aggregated in charging stations (CSs) and controlled by CS aggregators to follow the automatic generation control signals [10], [11].

V2G is being progressively integrated with primary frequency regulation and other active frequency support strategies under extreme grid disturbances [12]. Due to the inherent complexity of modeling and controlling V2G FR, particularly under the SFR framework, model predictive control (MPC) has emerged as a promising coordination strategy. Its ability to handle multi-timescale dynamics, system constraints, and predictive decision-making makes it well-suited for managing the charging and discharging of multiple EVs [13]. The uncertainty of EVs is often simplified as a state-of-charge (SoC) boundary [14] in MPC. Adaptive MPC can overcome the uncertainty of SoC ranges of EV [15]. MPC is used in [16] and [17] to improve grid dynamics and microgrid performance in frequency recovery. The inertial and droop characteristics are modelled by MPC to regulate EVs in [18]. In [19], MPC is combined with a virtual synchronous generator (VSG) for V2G FR and virtual inertia. Dis-

Manuscript received: August 19, 2025; revised: November 22, 2025; accepted: March 3, 2026. Date of CrossCheck: March 3, 2026. Date of online publication: April 1, 2026.

This work was supported by the National Natural Science Foundation of China (No. 52207229), Photonics Research Institute Strategic Grant (No. P0050885), the Key Research and Development Program of Ningxia Hui Autonomous Region of China (No. 2024BEE02003), and PolyU Startup Fund (No. P0052962).

S. Ke (corresponding author), J. Tian, R. Guo, S. He, and C. Y. Chung are with the Department of Electrical and Electronic Engineering and the Research Centre for Grid Modernisation, The Hong Kong Polytechnic University, Hong Kong, China (e-mail: song.ke@polyu.edu.hk; ruohan.guo@polyu.edu.hk; jinpeng.tian@polyu.edu.hk; shangyang.he@polyu.connect.hk; c.y.chung@polyu.edu.hk).

W. Mai is with Shenzhen Auto Electric Power Plant Co., Ltd., Shenzhen, China (e-mail: maiweijie@hotmail.com).

DOI: 10.35833/MPCE.2025.000759

tributed MPC (DMPC) strategy has shown its success in distribution networks for aggregated heterogeneous thermostatically loads [20] and demand response [21]. Therefore, the DMPC strategy allows the CS to make decentralized decisions independently, reducing the need for information exchange and protecting privacy.

Within MPC for V2G, a state-space model of the EV and V2G system must be established. V2G operation typically encompasses multiple components including the converter, the EV, and the power grid. Inappropriate model of V2G control may even introduce oscillatory behavior during grid frequency restoration [22]. While the AC/DC inverters of EV chargers are modeled in both [23] and [24], V2G inverters are also incorporated into the MPC-based FR framework in [19], where EV demands are modeled based on SoC constraints.

However, SoC is often the sole constraint considered in existing V2G research, while other internal battery states are neglected. In the battery equivalent circuit, parameters such as internal resistance and capacitance vary nonlinearly with SoC and influence charging/discharging dynamics. Consequently, if the V2G scheduling layer does not account for these internal battery states, V2G FR power commands may conflict with the battery management system (BMS), risking voltage or current violations and limiting safe and practical implementation.

Therefore, accurate prediction of the internal battery states is critical for effective MPC in FR control of V2G during grid disturbances. The charging/discharging rates and safety constraints of batteries, including voltage, current, and SoC limits, restrict their feasible operation region [25]. Neglecting these factors can result in overstressed battery operation, adversely affecting both its lifespan and operation safety. The FR power of battery is constrained by SoC and ramp-rate limits in [26]. The FR model in [27] considers the life-induced operation cost and the service quality. The resistor-capacitor (RC) equivalent circuit model (ECM) for batteries in [28] simplifies internal electrochemical dynamics while ensuring accuracy and computational efficiency, making it well-suited for FR in V2G applications [29]. The RC ECM of batteries and its parameters play a crucial yet often overlooked role in the design and implementation of V2G control strategy (Problem 1). In addition, the impact of V2G operation on battery degradation is experimentally quantified in [30], highlighting that battery degradation is a non-negligible factor in the V2G control strategy. Most existing MPC control strategies lack explicit battery state and degradation-aware modeling, which limits their ability to predict internal battery states, enforce operation constraints, and consider battery degradation. This limitation compromises the reliability and effectiveness of V2G FR (Problem 2).

Inspired by the above discussion, in this paper, the FR control of V2G leverages a DMPC strategy to construct a coordinated control strategy for EVs in the CS. In contrast to existing approaches, this paper explicitly integrates the battery state and degradation awareness for V2G FR, hence the proposed DMPC strategy enables a more realistic and responsive provision during FR. Specifically, battery power limits and SoC constraints are incorporated into the proposed DMPC strategy. This ensures that the BMS is tightly integrated with the V2G control strategy, allowing coordinated execution of V2G FR while maintaining battery operability and converter compliance with power commands. The main contributions of this paper are summarized as follows.

1) In response to Problem 1, we integrate an RC ECM of batteries into V2G FR, enabling the controller to accurately capture internal battery signals such as voltage and current. This improves the physical fidelity of the predictive model and ensures practical implementability, with a tracking deviation maintained below 3 kWs over a 20 s simulation period.

2) In response to Problem 2, we design an equivalent degradation model of batteries for the proposed DMPC strategy, allowing the controller to account for the degradation factor of EVs participating in V2G FR. The battery state and degradation awareness improve degradation preservation by more than 4.5%, ensuring safer and more sustainable battery operation.

3) We propose a cross-scale hierarchical framework for V2G control strategy, achieving hierarchical optimization across individual EVs and the CS. Simulation results demonstrate an improvement in FR performance, reducing frequency settling time by 6.5 s and providing more balanced V2G FR power allocation among EVs.

The remainder of this paper is organized as follows. In Section II, the problem formulation and preliminaries are presented. Section III details methodology. In Section IV, the case study is presented. Finally, conclusions are drawn in Section V.

II. Problem Formulation and Preliminaries

A. Problem Formulation in V2G FR

Existing V2G control strategy within SFR and LFC commonly adopts first-order inertial models and enforces V2G FR power constraints through hard bounds on SoC and power, which oversimplifies the underlying battery dynamics [31]. This strategy fails to adequately capture the heterogeneous limitations of individual EVs in the CS, due to variations in their battery states and operation constraints. Such shortcomings may result in power limit violations or suboptimal power allocation, adversely affecting both the effectiveness of frequency regulation and the efficiency of V2G settlements.

Thus, we focus on the challenges of real-time implementation for V2G control strategy in FR, particularly those arising from the lack of detailed battery modelling and operation constraints.

B. Preliminaries of LFC in Islanded Microgrid

In this context, we revisit the role of internal battery states in V2G FR. As shown in (1) and (2), V2G contributes to grid FR by adjusting charging and discharging power in real time.

$$\begin{cases} \Delta \dot{f}(t) = -\dfrac{D}{M}\Delta f(t) + \dfrac{1}{M}\Delta P_{\mathrm{CS}}(t) + \dfrac{1}{M}\Delta P_{\mathrm{G}}(t) + \dfrac{1}{M}\Delta P_{\mathrm{d}} \\ \Delta P_{\mathrm{d}}(t) = \Delta P_{\mathrm{WT}}(t) + \Delta P_{\mathrm{PV}}(t) - \Delta P_{\mathrm{L}}(t) \\ \Delta P_{\mathrm{CS}}(t) = \sum_{i=1}^{N} \Delta P_{\mathrm{EV}i}(t) \end{cases} \tag{1}$$

$$\Delta \dot{P}_{\mathrm{G}}(t) = \frac{1}{T_{\mathrm{G}} R_{\mathrm{G}}}\Delta f(t) - \frac{1}{T_{\mathrm{G}}}\Delta P_{\mathrm{G}}(t) \tag{2}$$

where t is the time instant; $\Delta f(t)$ is the frequency deviation; M and D are the inertia and damping of islanded microgrid, respectively; T_{G}, R_{G}, and ΔP_{G} are the deviations of time constant, droop coefficient, and output power of the microturbine, respectively; $\Delta P_{\mathrm{WT}}(t)$, $\Delta P_{\mathrm{PV}}(t)$, and $\Delta P_{\mathrm{L}}(t)$ are the deviations of wind power output, photovoltaic (PV) power output, and load power demand, respectively; $\Delta P_{\mathrm{EV}i}$ is the V2G FR power of the i^{th} EV; $\Delta P_{\mathrm{d}}(t)$ is the total disturbance power; $\Delta P_{\mathrm{CS}}(t)$ is the aggregated V2G FR; and N is the number of controllable EVs in the CS.

During this process, as illustrated in Fig. 1, the battery and BMS must coordinate with the DC/DC converter to deliver the required V2G FR power. The internal battery states (e.g., SoC, current, voltage) affect the parameters in the RC ECM of batteries, thereby constraining the available charging/discharging power P_{EV} and the dynamics of FR. The charging/discharging of each EV is managed by its local DMPC controller, and the distributed DMPC controllers exchange state information via a communication network to coordinate control decisions, which in turn directly influence the frequency regulation performance of islanded microgrid. This highlights the interaction between the battery model and the overall frequency control of islanded microgrid.

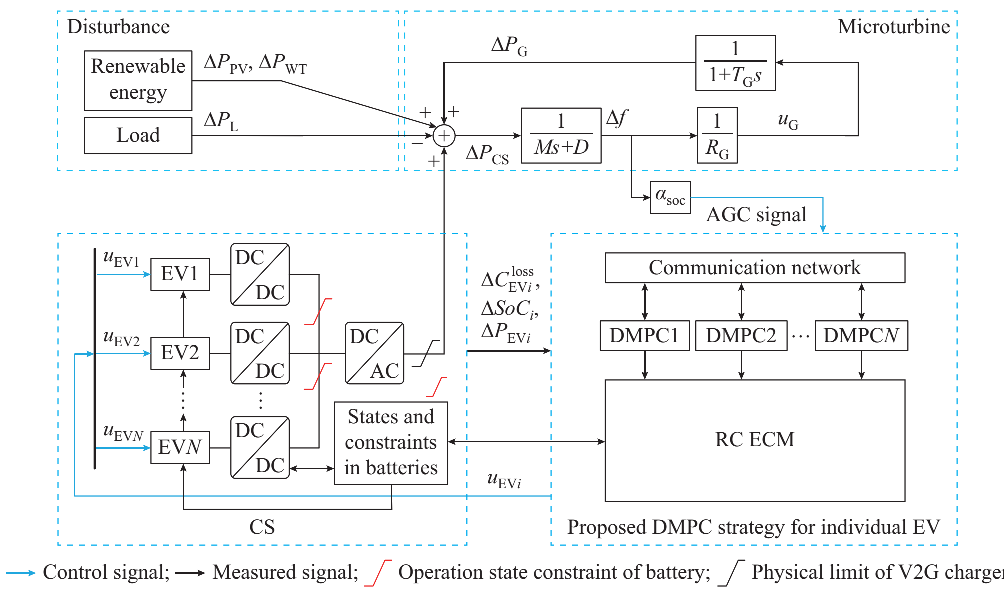

Fig. 1. SFR framework of frequency regulation for islanded microgrid.

The state-space model of frequency regulation of islanded microgrid, including CS, is developed using the method presented in [32]. Then, the SFR framework for frequency regulation of islanded microgrid is shown in Fig. 1. $u_{\mathrm{EV}i}$ $i = 1, 2, \ldots, N$ is the control input of the i^{th} EV produced by the proposed DMPC strategy; $\Delta C_{\mathrm{EV}i}^{\mathrm{loss}}$ and ΔSoC_i are the deviation of battery degradation rate and change of SoC of the i^{th} EV, respectively; and α_{soc} is the coordinated coefficient between different SoCs and the V2G FR power. The battery model for V2G is shown in Fig. 2 and its RC ECM is also introduced. Note that the variables in Fig. 2 are defined in the following equations.

The V2G FR power in the CS is constrained by battery states. The constraints of batteries are incorporated into the proposed DMPC strategy to facilitate EV participation in FR, as discussed in Section III. The frequency for islanded microgrid and the regulation power of the microturbine are regarded as globally accessible state variables within the proposed DMPC strategy for each EV.

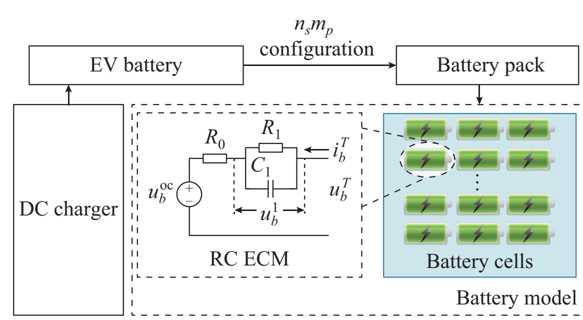

Fig. 2. Battery model for V2G.

III. Methodology

To address the above issue, a state-space EV model based on an RC ECM is developed, with an equivalent degradation model of batteries incorporated. The state-space EV model in the proposed DMPC strategy improves EV state predictions within the control horizon. By treating battery states as operation constraints, the proposed DMPC strategy ensures a more reasonable power allocation and prevents constraint violations.

A. RC ECM of Batteries

Existing V2G studies often neglect the battery states, remaining disconnected from the BMS. The RC ECM is used to capture the key dynamic characteristics of batteries such as transient voltage response while balancing modeling accuracy and computational efficiency. Therefore, we incorporate the RC ECM of batteries into the proposed DMPC strategy for V2G FR.

As shown in Fig. 2, the battery pack of an EV typically consists of multiple battery cells connected in series and parallel [29]. $n_s m_p$ denotes a battery pack with n battery cells connected in series and m battery cells connected in parallel per series string. The overall battery model can be constructed by aggregating voltage, current, and power according to the series-parallel configuration of the pack. The derivation process is described by:

$$u_b^T(t) = u_b^{\mathrm{oc}}(t) + u_b^1(t) + i_b^T(t) R_0(t) \tag{3}$$

where the superscript T refers to the physical quantities measured or defined at the external terminals of the battery or EV system; the subscript b denotes the index of battery cell; $u_b^T(t)$ is the terminal voltage of battery cell; $u_b^{\mathrm{oc}}(t)$ is the open-circuit voltage; $u_b^1(t)$ is the voltage across the RC parallel network (typically modeling transient response); $i_b^T(t)$ is the terminal current of battery cell, and $i_b^T(t) > 0$ indicates charging while $i_b^T(t) < 0$ indicates discharging; and $R_0(t)$ is the instantaneous ohmic resistance.

$u_b^1(t)$ is governed by the following differential equation as:

$$\frac{\mathrm{d}u_b^1(t)}{\mathrm{d}t} = -\frac{1}{R_1(t)C_1(t)} u_b^1(t) + \frac{1}{C_1(t)} i_b^T(t) \tag{4}$$

where $R_1(t)$ and $C_1(t)$ are the state-varying resistance and capacitance of the RC branch, respectively. Equation (4) captures the transient response of the battery cells due to charge redistribution and internal electrochemical processes, and it plays a critical role in accurately predicting the terminal voltage.

The parameters of the RC ECM such as resistances and capacitances influence the dynamic voltage response and thus constrain the available charging/discharging power, directly affecting the performance of the proposed DMPC strategy for V2G FR in frequency regulation of islanded microgrid. The parameters of the RC ECM at various SoCs can be identified through experiments on individual battery cells. In this paper, the identified parameter results of R_0, R_1, C_1, u_b^{oc} are denoted as $f_{R_0}, f_{R_1}, f_{C_1}, f_{u_b^{\mathrm{oc}}}$, respectively. The specific results are in [33], and the methodology is adapted as:

$$\begin{cases} R_0(t) = f_{R_0}\left[i_b^T(t), SoC(t)\right] \\ R_1(t) = f_{R_1}\left[i_b^T(t), SoC(t)\right] \\ C_1(t) = f_{C_1}\left[i_b^T(t), SoC(t)\right] \\ u_b^{\mathrm{oc}}(t) = f_{u_b^{\mathrm{oc}}}\left[i_b^T(t), SoC(t)\right] \end{cases} \tag{5}$$

where $SoC(t)$ is the charging/discharging SoC. The detailed definition of $SoC(t)$ is given as:

$$SoC(t) = SoC_{ini} + \frac{\eta_b}{3600 Q_0} \int_0^t i_b^T(\tau) u_b(\tau) \mathrm{d}\tau \tag{6}$$

where SoC_{ini} is the initial SoC of the EV participating in V2G FR; Q_0 is the rated capacity of the battery cell; η_b is the energy efficiency, and when $i_b^T(\tau) > 0$, η_b is set to be 1, and when $i_b^T(\tau) < 0$, η_b is set to be 0.98 to account for typical energy losses in the discharging process; τ is the integration element; and the integral term $i_b^T(\tau) u_b(\tau)$ represents the accumulated terminal power.

Equation (6) is derived from the energy balance and describes the variation in the battery state of energy. Within the modeling accuracy considered in this paper, this energy-based representation serves as an approximate SoC for system-level energy flow analysis.

The real-time adjustment of energy level $e_b^T(t)$ and power $p_b^T(t)$ of the battery cell can be expressed as:

$$\begin{cases} \dfrac{\mathrm{d}e_b^T(t)}{\mathrm{d}t} = p_b^T(t) \\ p_b^T(t) = u_b^T(t) i_b^T(t) \end{cases} \tag{7}$$

The energy level and terminal current of the battery cell are constrained by (8) and (9), respectively.

$$E_b^{T,\min} \le e_b^T(t) \le E_b^{T,\max} \tag{8}$$

$$\frac{-R_b^- Q_0}{u_{b\mathrm{nom}}^T} \le i_b^T(t) \le \frac{R_b^+ Q_0}{u_{b\mathrm{nom}}^T} \tag{9}$$

where $E_b^{T,\min}$ and $E_b^{T,\max}$ are the minimum and maximum allowable energy levels of the battery cell, respectively; R_b^+ and R_b^- are the maximum allowable discharging and charging C-rates, respectively; and $u_{b\mathrm{nom}}^T$ is the nominal voltage of the battery cell.

The RC ECM of batteries in (3)-(9) describes the internal states of the battery cell and characterizes the relationship among voltage, current, and circuit parameters within an individual battery cell. The RC circuit balances an accurate representation of battery states with computational efficiency. This model also explicitly updates the states of voltage, current, and circuit parameters. Incorporating this model into the V2G control strategy enables accurate state and constraint-aware power dispatch, particularly in real-time FR scenarios.

The battery pack consists of multiple cylindrical battery cells connected in series and parallel. Consequently, the total charging power $P_{\mathrm{EV}}(t)$ and energy $E_{\mathrm{EV}}(t)$ are formulated as the sums of the corresponding quantities of $p_b^T(t)$ and $e_b^T(t)$ in individual battery cells, as given in (10) and (11), respectively.

$$P_{\mathrm{EV}}(t) = \sum_{b \in B} p_b^T(t) \tag{10}$$

$$E_{\mathrm{EV}}(t) = \sum_{b \in B} e_b^T(t) \tag{11}$$

where B is the set of all battery cells within the battery pack.

Therefore, the battery model is constructed based on the RC ECM of individual battery cells and the pack structure. This model determines the states of internal voltage and current and provides the external V2G FR power. Establishing such a model enables seamless integration with V2G control strategy and achieves battery-state awareness. In the proposed DMPC strategy, the RC ECM allows each EV to accurately respond according to its own battery state and coordinated decisions among EVs, enabling reasonable power allocation to support frequency regulation of islanded microgrid while ensuring battery safety.

B. Equivalent Degradation Model of Batteries

Distributed EVs in the CS have heterogeneous battery states and interact with the grid through V2G. This interaction induces battery degradation and affects coordination control. Therefore, to account for battery degradation caused by EV FR, an equivalent degradation model of batteries is established. Based on an empirical degradation model and parameters in [34], the battery degradation $C_{\mathrm{EV}i}^{\mathrm{loss}}$ is given as:

$$C_{\mathrm{EV}i}^{\mathrm{loss}}=B_{cyc}\exp\left(\frac{-Ea_{cyc}+\alpha_{cyc}\left|i_b^T\right|}{R_gT_r}\right)\cdot Ah^{z_{cyc}} \tag{12}$$

where Ea_{cyc} is an activation energy for cycle aging expressed in 31700 J/mol; z_{cyc} is an exponent constant that should be around 0.5 for diffusion limited process; α_{cyc} is set to be 370.3 in cycling aging; R_g is the universal gas constant; T_r is the absolute temperature in Kelvin; Ah denotes the cumulative charge passed through a battery over its life, either during charging or discharging period; and B_{cyc} is a pre-exponential factor in $Ah^{1-z_{cyc}}$ that depends on current.

To make (12) suitable for different operation conditions, (12) has been differentiated against time in (13), denoted as $\Delta C_{\mathrm{EV}i}^{\mathrm{loss}}$, to evaluate battery degradation rate due to V2G FR.

$$\Delta C_{\mathrm{EV}i}^{\mathrm{loss}}=\frac{\mathrm{d}C_{\mathrm{EV}i}^{\mathrm{loss}}}{\mathrm{d}t}=\frac{\left|i_b^T\right|}{3600}z_{cyc}B_{cyc}(I)\exp\left(\frac{-Ea_{cyc}+\alpha_{cyc}\left|i_b^T\right|}{R_gT_r}\right)\cdot\left(\frac{C_{\mathrm{EV}i}^{\mathrm{loss}}}{B_{cyc}(I)\exp\left(\dfrac{-Ea_{cyc}+\alpha_{cyc}\left|i_b^T\right|}{R_gT_r}\right)}\right)^{1-\frac{1}{z_{cyc}}} \tag{13}$$

Given that EV FR occurs over a short timescale, variations in parameters such as R_g and T_r are neglected. Accordingly, (13) is employed to describe the real-time battery degradation rate during the FR process as it offers higher accuracy than (12).

During participation in V2G FR, the battery degradation rate is evaluated using (13), serving as a key reference for power allocation in the DMPC-based FR control. As this evaluation involves current and energy, the RC ECM of batteries in (3)-(11) is embedded into the proposed DMPC strategy to facilitate accurate state prediction and effective integration of battery degradation awareness.

C. State-space EV Model Based on ECM

As shown in Supplementary Material A Fig. SA1, a model for V2G control strategy in FR is first established to incorporate the battery state and related constraints into the state-space model, and we define this model as V2G control model.

In this model, the coupled real-time interaction between the battery model and the V2G control system is investigated. The details of the state-space EV model can be found in Supplementary Material A.

To facilitate MPC computation, the state-space EV model is discretized. The dynamic behavior of $u_b^1(t)$ is discretized as:

$$\begin{cases} u_b^1(k+1)=u_b^1(k)\mathrm{e}^{-\frac{\Delta t}{\tau_1(k)}}+i_b^T(k)R_1(k)\left(1-\mathrm{e}^{-\frac{\Delta t}{\tau_1(k)}}\right) \\ \tau_1(k)=R_1(k)C_1(k) \end{cases} \tag{14}$$

where k is the discrete time step index; and Δt is the time interval between two consecutive sampling instants.

In addition to the execution of the proposed DMPC strategy, it is essential to clarify the process and principles of battery state updating. To track the power commands assigned to the EV, the output power is composed of the aggregated contributions from all battery cells within the battery pack. The terminal voltage of each battery cell is determined by (3) and (4). To abstract the complexity of the power converter, a proportional-integral (PI) current control loop is employed according to (15).

$$i_{b,i}^T(k+1)=PI\left[P_{\mathrm{EV}i}^{\mathrm{ref}}(k)-P_{\mathrm{EV}i}(k)\right]=i_{b,i}^T(k)+K_P\Delta P_{\mathrm{EV}i}^{\mathrm{dev}}(k)+K_I\sum_{\tau=0}^{k}\Delta P_{\mathrm{EV}i}^{\mathrm{dev}}(\tau)\Delta t \tag{15}$$

where the subscript i denotes the i^{th} EV in the CS; $P_{\mathrm{EV}i}^{\mathrm{ref}}$ is the reference EV power from the controller; $P_{\mathrm{EV}i}$ is the EV power predicted by the battery model; K_P and K_I are the proportional and integral gains, respectively; and $\Delta P_{\mathrm{EV}i}^{\mathrm{dev}}$ is the deviation of EV power predicted by the battery model.

To explicitly account for power tracking performance and dynamic response, and further mitigate its impact on FR, $\Delta P_{\mathrm{EV}i}^{\mathrm{dev}}(k)$ is introduced as a state variable.

$$\Delta P_{\mathrm{EV}i}^{\mathrm{dev}}(k)=P_{\mathrm{EV}i}^{\mathrm{ref}}(k)-P_{\mathrm{EV}i}(k) \tag{16}$$

$\Delta P_{\mathrm{EV}i}^{\mathrm{dev}}(k)$ between $P_{\mathrm{EV}i}^{\mathrm{ref}}(k)$ and $P_{\mathrm{EV}i}(k)$ functions both as an output deviation indicator and as a state variable within the DMPC to enable accurate prediction and optimization of V2G FR power in the proposed DMPC strategy. The V2G FR power modeling based on battery states is detailed in Supplementary Material A Fig. SA2. Unlike existing approaches that treat power and SoC as hard constraints, we further incorporate BMS-level current and voltage limits, forming dual constraints on V2G FR power. This ensures reliable DMPC execution. Together, the V2G control model and power response model in Supplementary Material A Figs. SA1 and SA2 establish a unified link between battery states and V2G FR power while accounting for states and constraints of the battery from V2G participation.

The V2G control model incorporating battery states can be integrated into the SFR framework of islanded microgrid with V2G FR, as illustrated in Fig. 3.

This V2G control model serves as the prediction model for the proposed DMPC strategy, extending conventional converter constraints by including battery state limitations to ensure safe and reliable control. The detailed derivation of the state-space EV model is presented as follows.

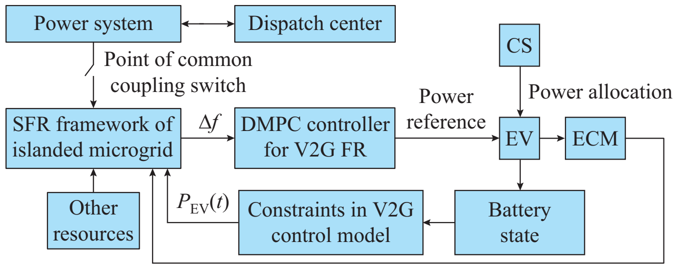

Fig. 3. Location of battery states in SFR framework of islanded microgrid with V2G FR.

Based on (16), the V2G FR power model of the i^{th} EV in the CS considering battery states and constraints is derived and presented in (17) and Supplementary Material A Fig. SA2. $\Delta P_{\mathrm{EV}}^{\mathrm{dev}}(t)$ is used as an index to characterize the dynamic response process of the EVs. This V2G FR power model can be used to analyze the FR process of EVs with respect to their battery management.

$$\Delta \dot{P}_{\mathrm{EV}i}^{\mathrm{dev}}(t)=\frac{\partial \Delta P_{\mathrm{EV}i}^{\mathrm{dev}}(t)}{\partial P_{\mathrm{EV}i}^{\mathrm{ref}}(t)}\Delta P_{\mathrm{EV}i}^{\mathrm{ref}}(t)+\frac{\partial \Delta P_{\mathrm{EV}i}^{\mathrm{dev}}(t)}{\partial U_{\mathrm{EV}i}(t)}\Delta U_{\mathrm{EV}i}(t) \tag{17}$$

where $U_{\mathrm{EV}i}(t)$ and $\Delta U_{\mathrm{EV}i}(t)$ are the terminal voltage and its deviation of the battery pack, respectively.

The objective of the DMPC controller is to take the state variables and the designed communication states of each EV as inputs for coordination, and generate the corresponding $\Delta P_{\mathrm{EV}i}^{\mathrm{ref}}(t)$ for each EV. Hence, FR support is provided, minimizing the mismatch between $P_{\mathrm{EV}i}(t)$ and $P_{\mathrm{EV}i}^{\mathrm{ref}}(t)$ and mitigating battery degradation during the FR process.

Therefore, a state-space EV model and corresponding DMPC controller are designed for each EV. The state vector of the EV incorporates $\Delta P_{\mathrm{EV}i}(t)$, the deviation of delayed coordination control input received by the i^{th} EV from the j^{th} EV $\Delta u_{\mathrm{EV}ij}^{\mathrm{delay}}(t)$, the deviation of SoC of the i^{th} EV $\Delta SoC_i(t)$, and $\Delta C_{\mathrm{EV}i}^{\mathrm{loss}}$ in (13). Equation (13) is nonlinear and serves to quantify and compare the differential impact of V2G FR power on cycle-induced loss of battery capacity. It is linearized using a Taylor series expansion. In order to ensure the reasonable allocation of response power among the EVs while protecting the information privacy among them, only the SoC is exchanged among the EVs. The response power of the i^{th} EV is influenced both by the output of its own DMPC controller as the command and by the coordinated component. The battery state update in the EV is considered in the state equations. To reduce the complexity of the solution, the SoC information of other EVs is differenced and treated as a coordination term, which is incorporated into the control model of each EV. Additionally, the individual battery degradation is set as the control objective of the DMPC. The state equations are given in Supplementary Material A.

Therefore, a discrete state-space EV model is established for each EV within the CS.

$$\begin{cases} \boldsymbol{x}_{\mathrm{EV}i}(k+1)=\boldsymbol{A}_{\mathrm{EV}i}\boldsymbol{x}_{\mathrm{EV}i}(k)+\boldsymbol{B}_{\mathrm{EV}i}\boldsymbol{u}_{\mathrm{EV}i}(k)+ \\ \qquad \sum\limits_{i\neq j}\left(\boldsymbol{L}_{\mathrm{EV}ij}\boldsymbol{A}_{\mathrm{EV}ij}\boldsymbol{x}_{\mathrm{EV}j}(k)+\boldsymbol{B}_{\mathrm{EV}j}\boldsymbol{u}_{\mathrm{EV}j}(k)\right) \\ \boldsymbol{y}_{\mathrm{EV}i}(k)=\boldsymbol{C}_{\mathrm{EV}i}\boldsymbol{x}_{\mathrm{EV}i}(k) \end{cases} \tag{18}$$

where $\boldsymbol{x}_{\mathrm{EV}i}=\left[\Delta f(t),\ \Delta P_{\mathrm{G}}(t),\ \Delta P_{\mathrm{EV}i}^{\mathrm{dev}}(t),\ \Delta u_{\mathrm{EV}ij}^{\mathrm{delay}}(t),\ \Delta SoC_i(t),\ \Delta C_{\mathrm{EV}i}^{\mathrm{loss}}(t)\right]^{\mathrm{T}}\in\mathbb{R}^{n_{\mathrm{ev}}}$ with $\mathbb{R}^{n_{\mathrm{ev}}}$ indicating n_{ev}-dimensional real Euclidean space; $\boldsymbol{y}_{\mathrm{EV}i}=\left[\Delta f(t),\Delta P_{\mathrm{EV}i}^{\mathrm{dev}}(t),\Delta SoC_i(t),\Delta C_{\mathrm{EV}i}^{\mathrm{loss}}(t)\right]^{\mathrm{T}}$; $\boldsymbol{A}_{\mathrm{EV}ij}$ is the state-coordinated communication matrix from the j^{th} EV to the i^{th} EV; $\boldsymbol{u}_{\mathrm{EV}i}(t)$ is the output increment vector of the i^{th} EV; $\boldsymbol{A}_{\mathrm{EV}i}$ is the discrete-time state transition matrix of the i^{th} EV; $\boldsymbol{B}_{\mathrm{EV}i}$ is the control input matrix of the i^{th} EV; $\boldsymbol{L}_{\mathrm{EV}ij}$ is the communication link matrix of the j^{th} EVs to the i^{th} EV, and it is a 0-1 square matrix whose dimension corresponds to the number of controllable EVs; and $\boldsymbol{C}_{\mathrm{EV}i}$ is the output matrix of the i^{th} EV.

State collaboration among EVs is implemented as follows. In addition to monitoring the frequency of islanded microgrid, information exchange between EVs is limited to SoC, with no other state variables transmitted. If a communication link exists between the i^{th} and the j^{th} EVs, $\boldsymbol{A}_{\mathrm{EV}ij}$ is defined, with details shown in Supplementary Material A; otherwise, it is set to be a zero matrix. This design reduces communication burden and enhances user privacy.

In this paper, we construct the V2G control model, which is capable of sensing battery states, interfacing with both the BMS and the V2G system. The resulting state-space EV model can be integrated into the state-space framework of the DMPC controller for individual EVs.

D. Proposed DMPC Strategy with Battery State Constraints for LFC

The future states and predicted outputs of all controlled EVs within the prediction horizon are derived from (18).

$$\begin{cases} \bar{\boldsymbol{x}}_{\mathrm{EV}i}\left(k+N_p+1|k\right)=\boldsymbol{A}_{\mathrm{CS}}^{N_p}\boldsymbol{L}_i\boldsymbol{X}_{\mathrm{CS}}(k)+\boldsymbol{A}_{\mathrm{CS}}^{N_p}\boldsymbol{L}_i'\bar{\boldsymbol{X}}_{\mathrm{CS}}\left(k|k-1\right)+ \\ \qquad \sum\limits_{s=1}^{N_p}\boldsymbol{A}_{\mathrm{CS}}^{s-1}\boldsymbol{B}_{\mathrm{EV}i}\boldsymbol{u}_{\mathrm{EV}i}\left(k+s|k\right)+ \\ \qquad \sum\limits_{j\neq i,j\in\{1,2,\dots,N\}}\sum\limits_{s=1}^{N_p}\boldsymbol{A}_{\mathrm{CS}}^{s-1}\boldsymbol{B}_{\mathrm{EV}j}\boldsymbol{u}_{\mathrm{EV}j}\left(k+s|k-1\right) \\ \bar{\boldsymbol{y}}_{\mathrm{EV}i}\left(k+N_p+1|k\right)=\boldsymbol{C}_{\mathrm{EV}i}\bar{\boldsymbol{x}}_{\mathrm{EV}i}\left(k+N_p+1|k\right) \end{cases} \tag{19}$$

where s is the number of fixed prediction steps; N_p is the length of prediction horizon; $\boldsymbol{X}_{\mathrm{CS}}$ is the steady-state vector of EVs; $\boldsymbol{A}_{\mathrm{CS}}^{N_p}$ is the dynamic adjustment state vector of EVs; $\boldsymbol{L}_i$ is the local weight vector of the i^{th} EV; $\boldsymbol{L}_i'$ is the neighboring coupling weight vector of the i^{th} EV; and $^-$ denotes the corresponding predicted value. Each EV executes its own DMPC controller, computing its future input $\boldsymbol{u}_{\mathrm{EV}i}\left(k+s|k\right)$ for a fixed prediction step s. Note that $\boldsymbol{X}_{\mathrm{CS}}$, $\boldsymbol{A}_{\mathrm{CS}}$, $\boldsymbol{L}_i$, and $\boldsymbol{L}_i'$ are further illustrated in Supplementary Material A (SA1)-(SA4).

Based on the controller output, the states of each EV can be updated, and future states can be predicted. As the DMPC controller is employed for each EV, the primary objective is to allocate the V2G FR power effectively, accelerate the frequency recovery of the islanded microgrid, reduce the output of the microturbine, and minimize the battery degradation. Since these control objectives are all related to the state variables in the EV state equations, the variation of the entire state vector is adopted as the optimization target. The multi-objective control problem, including V2G FR power and battery degradation, is coordinated through a weighting matrix to balance these control objectives. Therefore, the control objective of DMPC controller $J_{\mathrm{EV}i}$ designed for each EV at time k is formulated as:

$$J_{\mathrm{EV}i}(k)=\min\sum_{n=0}^{N_c}\Bigg(\left(\bar{\boldsymbol{x}}_{\mathrm{EV}i}(k+n|k)\right)^2_{\boldsymbol{Q}_i}+\left(\bar{\boldsymbol{u}}_{\mathrm{EV}i}(k+n|k)\right)^2_{\boldsymbol{R}_i}+\sum_{j=1,j\neq i}^{N}\left(\bar{\boldsymbol{u}}_{\mathrm{EV}j}(k+n|k-1)\right)^2_{\boldsymbol{R}_j}\Bigg) \tag{20}$$

where $\boldsymbol{Q}_i$, $\boldsymbol{R}_i$, and $\boldsymbol{R}_j$ are the positive definite and symmetric weighting matrices corresponding to the states, control inputs, and collaborative control inputs, respectively; and N_c is the control horizon that is set to be 10.

The cost function in (20) incorporates state variables such as frequency recovery of islanded microgrid, V2G FR power, power deviation, as well as the states representing coordination among multiple EVs. By tuning the associated weights, the cost function can balance these objectives, achieving an optimal coordination and desired control performance. The control constraints in the proposed DMPC strategy are given as:

$$\begin{cases} P_{\mathrm{EV}i,\max}^{\mathrm{cha}}\leq \Delta P_{\mathrm{EV}i}^{\mathrm{ref}}(k)\leq P_{\mathrm{EV}i,\max}^{\mathrm{dis}} \\ SoC_i^{\min}\leq SoC_i(k)\leq SoC_i^{\max} \\ u_{b,i}^T, i_{b,i}^T\in \Omega_{\mathrm{safe}} \end{cases} \tag{21}$$

where $P_{\mathrm{EV}i,\max}^{\mathrm{cha}}$ and $P_{\mathrm{EV}i,\max}^{\mathrm{dis}}$ are the maximum charging and discharging power of the i^{th} EV, respectively; and $SoC_i^{\min}$ and $SoC_i^{\max}$ are the minimum and maximum acceptable SoC limits for the i^{th} EV, respectively. Note that $u_{b,i}^T$ and $i_{b,i}^T$ must remain within safety boundaries Ω_{safe} to prevent overcharging.

The workflow of the proposed DMPC strategy is further illustrated in Supplementary Material A Fig. SA3. The DMPC controller receives the frequency deviation of the islanded microgrid, as shown in (1). Simultaneously, it collects outputs from all EVs within the CS, including SoC, V2G FR power, and the error between the actual V2G FR power from the BMS and that predicted by the state-space EV model, enabling real-time evaluation of the EV states and control effectiveness. Based on these inputs, the DMPC controller generates optimal power control commands for each EV, forming a cross-scale hierarchical framework for V2G control strategy.

IV. Case Study

A. Simulation Setup and Cases

In this paper, the state-space EV model with battery state and degradation awareness is incorporated into the predictive model of the DMPC controller for V2G FR. The simulation models used in this paper are the same as those employed for the DMPC controller and state observer design, ensuring the consistency between control design and simulation analysis. The battery model is based on an RC ECM [33], and the V2G control model follows the LFC modeling commonly used in FR control [19]. The objective is to ensure that the V2G FR satisfies the internal battery state constraints of EVs while enhancing the FR performance and improving the rationality of power allocation in the proposed DMPC strategy. Accordingly, in the simulation study, the effectiveness of the proposed DMPC strategy is evaluated by comparing different controllers and by employing various EV models within the controller. The control horizon of 10 steps is selected with a sampling time of 0.1 s, resulting in a prediction horizon of 1 s. The selected horizon provides a good balance, ensuring satisfactory tracking performance and stable operation while maintaining real-time feasibility.

The simulation is conducted in an islanded microgrid for frequency regulation, including a CS. The detailed parameters are given in Supplementary Material B Table SBI. The cost function weights are set to be [0.3, 0, 0.3, 0.1, 0, 0.3]. The weights for generator output and SoC variation are set to be zero to simplify the optimization, which is applicable to CSs with a larger number of EVs. However, for the sake of clarity in presenting the simulation results, 6 EVs in different SoC ranges are considered in the CS, with initial SoC values of 75%, 65%, 55%, 45%, 35%, and 25%, respectively. The fluctuations of wind and PV power or load are introduced as disturbances, with FR jointly provided by microturbines and the CS participating in V2G. A load disturbance is applied at 4 s, and the frequency recovery process is observed over a 20-s period. Three disturbance scenarios are considered, listed as follows.

1) Scenario 1: with step load disturbance of 0.1 p.u. at 4 s.

2) Scenario 2: with 0.1 p.u. step disturbance superimposed with ±0.08 p.u. stochastic fluctuation.

3) Scenario 3: with the same step disturbance as Scenario 1, used for comparison with other typical control strategies.

Note that Scenarios 1 and 2 are designed to evaluate the V2G FR capability to ① respond to sudden, large, and deterministic load changes, and ② maintain steady-state regulation and robustness under uncertain disturbances. Scenario 3 compares the proposed DMPC strategy with a centralized MPC and two model-free controllers including droop control ($R_{cs}=0.2$) and VSG control ($J=200$ and $D=120$) [24], where R_{cs} is the droop coefficient of CS; and J is the moment of inertia. The centralized MPC uses the same model and constraints without distributed coordination. Other settings and disturbances match those in Scenario 1.

In each scenario, four simulation cases are considered as follows.

1) Case 1: the proposed DMPC strategy (with communication among EVs) is adopted.

2) Case 2: centralized droop control (baseline strategy) is adopted.

3) Case 3: DMPC (without communication among EVs) is adopted.

4) Case 4: VSG control is adopted.

In Case 1, the battery model is incorporated into the DMPC controller, enabling accurate predictions of battery voltage and current, which are treated as state constraints. Apart from the specific differences, all other settings in Cases 2-4 are kept the same as those in Case 1. Case 2 adopts the centralized droop control, as shown in Fig. 4(a). Case 3 adopts the DMPC, as shown in Fig. 4(b), and neglects the communication among EVs, meaning that each EV within the CS operates its own independent MPC controller. Case 4 models each EV as a first-order inertial element, and its time constant $T_{EV}=0.5$ s. For Case 4, the battery model employed in Case 1 is replaced with a first-order inertia link to represent the dynamic response of the EV when executing power commands. The modeling of the first-order inertia link is consistent with other existing research [19] on V2G FR. However, the battery degradation rate is still calculated using (12) and (13) for comparison.

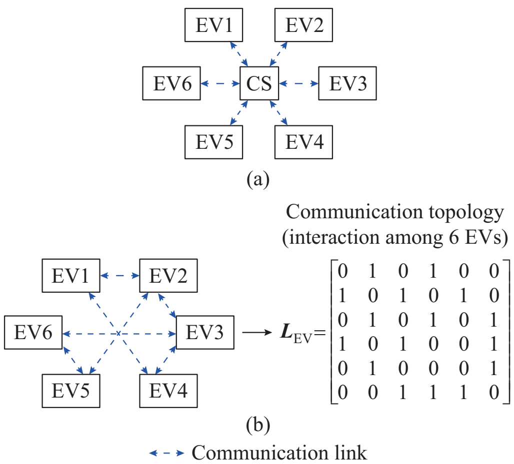

Fig. 4. Communication topology of coordinated EVs in Cases 1-4. (a) Centralized droop control. (b) DMPC.

B. Results and Discussions

The effectiveness of the proposed DMPC strategy is evaluated primarily from two perspectives: frequency recovery and execution of the V2G FR control. Frequency recovery is assessed using two metrics: the frequency nadir $\Delta f_{\mathrm{nadir}}$ and the frequency settling time T_{settle}. T_{settle} is defined when $\Delta f(t)$ first enters and subsequently remains within the absolute tolerance band of ±0.02 Hz:

$$T_{\mathrm{settle}}=\min\left\{t\geq 0\,\middle|\,\forall\tau\geq t,\left|\Delta f(\tau)\right|\leq 0.02\ \mathrm{Hz}\right\} \tag{22}$$

The execution of the proposed DMPC strategy is evaluated using four performance metrics: the cumulative frequency deviation $\int_t\sum_{i=1}^{N}\Delta P_{\mathrm{EV}i}^{\mathrm{dev}}(t)\,\mathrm{d}t$, the maximum output of the microturbine ΔP_{Gmax}, the cumulative battery degradation $\int_t\sum_{i=1}^{N}\Delta C_{\mathrm{EV}i}^{\mathrm{loss}}(t)\,\mathrm{d}t$, and the amount of information exchange Q_{comm}. $\int_t\sum_{i=1}^{N}\Delta P_{\mathrm{EV}i}^{\mathrm{dev}}(t)\,\mathrm{d}t$ and $\int_t\sum_{i=1}^{N}\Delta C_{\mathrm{EV}i}^{\mathrm{loss}}(t)\,\mathrm{d}t$ correspond to the definite integral of $\Delta P_{\mathrm{EV}i}^{\mathrm{dev}}$ in (16) and $\Delta C_{\mathrm{EV}i}^{\mathrm{loss}}$ in (13) of all EVs over the simulation interval, respectively. The state comparison of four cases in Scenario 1 is shown in Fig. 5. The amount of Q_{comm} is quantified using the bidirectional communication links and the collaborative interaction state variables, which is defined as:

$$Q_{\mathrm{comm}}=\begin{cases}N(N-1)\left(m_{\mathrm{states}}^{\mathrm{EV}}+m_{\mathrm{states}}^{\mathrm{global}}\right) & Q_{\mathrm{comm}}=Q_{\mathrm{comm}}^{\mathrm{center}}\\ \left(\sum_{i=1}^{N}\sum_{j=1}^{N}L_{\mathrm{EV}ij}\right)m_{\mathrm{states}}^{\mathrm{EV}}+2Nm_{\mathrm{states}}^{\mathrm{global}} & Q_{\mathrm{comm}}=Q_{\mathrm{comm}}^{\mathrm{dmpc}}\end{cases} \tag{23}$$

where $Q_{\mathrm{comm}}^{\mathrm{center}}$ and $Q_{\mathrm{comm}}^{\mathrm{dmpc}}$ are the total amounts of communications in the centralized droop controller and DMPC controller, respectively; $m_{\mathrm{states}}^{\mathrm{EV}}$ is the number of collaborative state variables of state-space EV model; $m_{\mathrm{states}}^{\mathrm{global}}$ is the number of global state variables in the proposed DMPC strategy including the frequency of islanded microgrid and microturbine output; and $L_{\mathrm{EV}ij}$ is the element of $\boldsymbol{L}_{\mathrm{EV}ij}$.

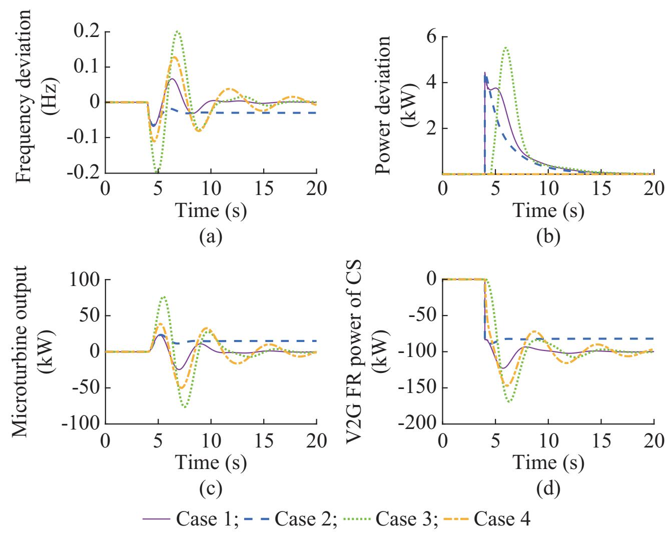

Fig. 5. State comparison of four cases in Scenario 1. (a) Frequency deviation. (b) Power deviation. (c) Microturbine output. (d) V2G FR power of CS.

The simulation presented in this paper is carried out using MATLAB R2024a and Simulink. The simulation results are analyzed separately for Scenario 1 and Scenario 2. Note that additional comparisons with other typical control strategies (as defined by Scenario 3) are provided in Supplementary Material C.

1) Scenario 1

The step disturbance primarily examines the transient response characteristics of the control strategy such as the frequency nadir, frequency settling time, and steady-state error. Therefore, in Scenario 1, following a step disturbance in 4 s, the EVs participating in V2G under the proposed DMPC strategy provide frequency support according to the control commands issued by the DMPC controller, jointly supporting the frequency alongside the microturbine in the islanded microgrid. The frequency deviation, power deviation, microturbine output, and V2G FR power of CS are illustrated in Fig. 5. By taking the first EV (EV1) as an example, the V2G FR power modeling for battery of EV1 in Case 1 of Scenario 1 is shown in Fig. 6. The quantitative metrics regarding frequency recovery performance and execution of the V2G FR control are summarized in Supplementary Material C Table SC1. Figures 5(b) and 6 jointly illustrate the role of the battery model within the proposed DMPC strategy.

As illustrated in Fig. 6, the battery states adhere to the imposed state constraints, effectively maintaining voltage and current within the safe operation region. The dynamic response of the battery model to power commands closely resembles a first-order inertial system, as commonly assumed in existing studies.

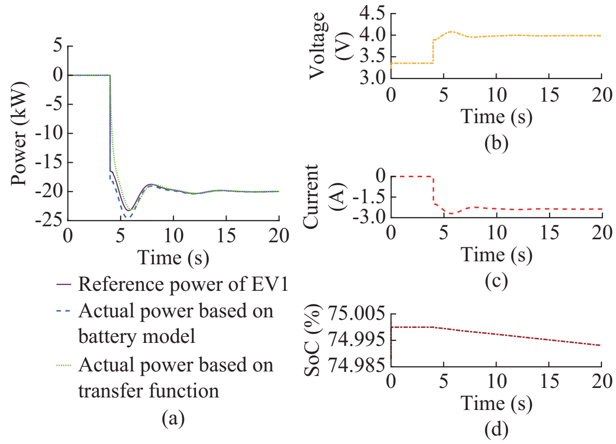

Fig. 6. V2G FR power modeling for battery of EV1 in Case 1 of Scenario 1. (a) Power. (b) Voltage. (c) Current. (d) SoC.

Owing to the inherent response delay of the closed-loop control system, a deviation between the power command and actual power is inevitable. However, this deviation diminishes gradually after approximately 3.7 s following the disturbance, once the power command becomes constant. The system frequency subsequently enters the stable region about 4.9 s after the disturbance, which is significantly shorter than those in Case 3 (6.2 s) and Case 4 (11.4 s), indicating the positive impact of incorporating battery state constraints on the FR performance of the DMPC controller.

Although the centralized droop control in Case 2 exhibits smaller oscillation amplitudes, it suffers from a steady-state frequency deviation of 0.03 Hz. The typical safe operation region is set to be 0.02 Hz, and such a steady-state frequency deviation is unacceptable. Centralized droop control features simple implementation, fast response, and robustness to model uncertainties, enabling direct local reaction to system disturbances. However, it struggles to handle complex operation constraints and offers low power allocation accuracy, being tied to predefined droop coefficients.

To further clarify the differences in control performance and communication architecture, we compare Case 1 and Case 2. The DMPC in Case 1 enables secondary frequency regulation and full frequency restoration, though its power commands may exhibit transient oscillations. In contrast, the centralized droop control in Case 2 stabilizes frequency deviations but cannot restore the frequency to its nominal value, providing only primary frequency control. Therefore, the power deviations in Case 1 are larger than those in Case 2, which is acceptable. Moreover, the centralized structure of Case 2 increases the number of links, reduces reliability, and raises privacy concerns, whereas the distributed structure of Case 1 reduces communication requirements and enhances scalability and data security, making it a more practical choice.

In Case 3, the communication among individual EVs is neglected, and each MPC controller lacks access to the actual power responses and states of other EVs. In Case 4, a first-order inertia element is employed for modeling, which makes it difficult to explicitly incorporate internal battery states and constraints into the DMPC controller. Moreover, the inherent delay of the first-order inertia element leads to a larger power deviation. As a result, both Case 3 and Case 4 exhibit more severe frequency oscillation amplitudes.

By taking Case 1 as an example, the power allocation results of individual EVs within the proposed DMPC strategy are presented. Due to variations in the SoC, the power allocation among EVs is illustrated in Fig. 7. Note that in Fig. 7, EVi_{ref} represents the reference power command generated by the DMPC controller for the i^{th} EV, while EVi_{real} represents the actual power output for the i^{th} EV considering the battery dynamics and constraints. Generally, EVs with higher SoC are allocated with larger power responses. However, the incorporation of power deviations of EV model within the DMPC controller results in a nonlinear relationship among SoC levels, power allocation, and power deviations. The metrics in Table SAII reveal that Case 1 demonstrates superior performance over Case 3 and Case 4 across multiple metrics, including $\Delta f_{\mathrm{nadir}}$, T_{settle}, $\int_t \sum_{i=1}^{N} \Delta C_{\mathrm{EV}i}^{\mathrm{loss}}(t)\,\mathrm{d}t$, and $\int_t \sum_{i=1}^{N} \Delta P_{\mathrm{EV}i}^{\mathrm{dev}}(t)\,\mathrm{d}t$. The results support that the proposed DMPC strategy combines the control objectives while coordinating the battery states and power responses of the individual EVs.

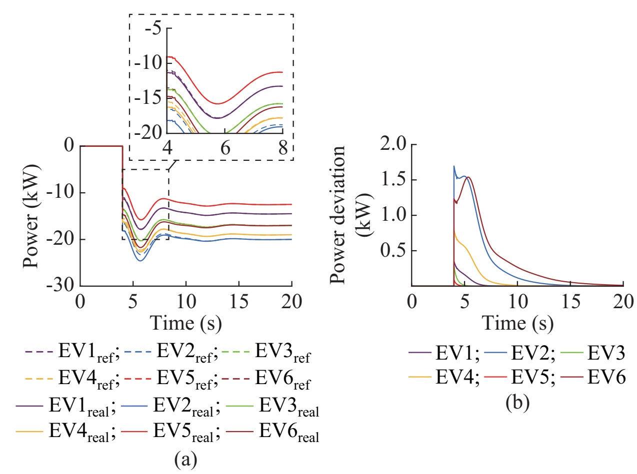

Fig. 7. Power allocation among EVs. (a) Power. (b) Power deviation.

2) *Scenario 2*

To evaluate the performance of the V2G control system with the battery model under realistic and unpredictable disturbances, Scenario 2 is designed with continuous random frequency fluctuations based on Scenario 1. Scenario 2 tests the robustness and dynamic regulation capability of the controller. Compared with the step disturbance scenario, continuous random frequency fluctuations impose more frequent and irregular control actions, which limit the effectiveness of EV coordination. The state comparison of four cases in Scenario 2 is shown in Fig. 8.

The frequency recovery trend is similar to that in Scenario 1, with the frequency nadir in Case 1 being 0.1359 Hz. In

Case 2, centralized droop control slightly improves frequency stability and attenuates oscillations. However, it still fails to address the challenges of complex model constraints, steady-state deviation, and optimal coordination of power allocation because of the control framework.

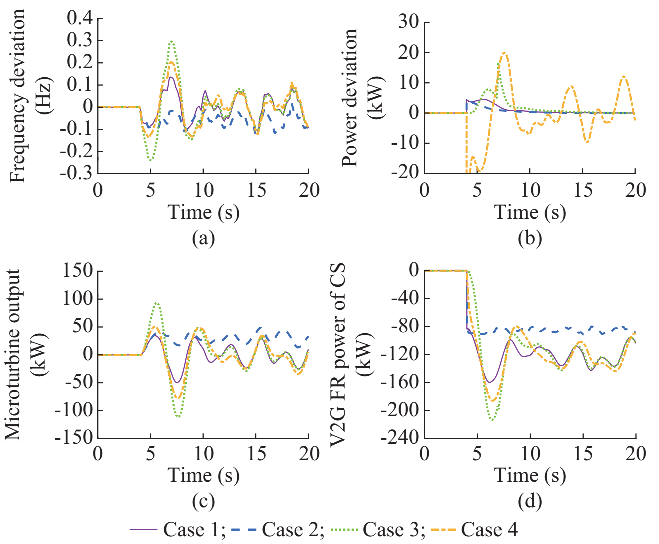

Fig. 8. State comparison of four cases in Scenario 2. (a) Frequency deviation. (b) Power deviation. (c) Microturbine output. (d) V2G FR power of CS.

Under random disturbances, Case 1 still outperforms Case 3 (0.2960 Hz) and Case 4 (0.2024 Hz) in frequency stability. This is because, in Case 3, the EVs lose their coordinated effects, and the share of microturbine output increases by 84.3% compared with that in Case 4, thereby reducing the V2G contribution. Due to the large inertia of the microturbine, the oscillation amplitude becomes more pronounced.

In Case 4, with the EVs modeled as first-order inertial elements, their V2G FR power cannot accurately track rapidly varying control commands under random disturbances, resulting in a significant power deviation. The accumulated deviation reaches −10.416 kWs, which is not considered in the control strategy design. Consequently, the first-order inertia modeling is inadequate for frequency regulation in the scenarios with high stochasticity.

The performance metrics are listed in Supplementary Material A Table SAII, along with detailed illustration. These metrics collectively reflect the dynamic performance, control efficiency, and communication requirements for different cases. From the results presented in Table SAII, it can be observed that in scenarios 1 and 2, Case 1 and Case 2 perform significantly better than Case 3 and Case 4 in the first four metrics, i.e., Δf_{nadir}, T_{settle}, $\int \sum_{i=1}^{N} \Delta P_{\text{EV}i}^{\text{loss}}(t)\,\mathrm{d}t$, and ΔP_{Gmax}, which highlights the effectiveness of the EV model for V2G control and the superiority of the proposed DMPC strategy. Furthermore, a comparison between Case 1 and Case 2 reveals that, while achieving nearly identical frequency response performance (the frequency nadir differs by only 0.001 Hz in Scenario 1 and 0.008 Hz in Scenario 2), Case 1 requires fewer communication links and a lower microturbine output. This indicates that Case 1 can achieve comparable frequency regulation performance with reduced communication and generation effort, thereby demonstrating a more efficient utilization of the V2G capability.

3) Battery Degradation Analysis

The battery model in this paper enables the calculation of the V2G FR power during the response process and the battery state variables. This model is applied consistently across all four cases in Scenarios 1 and 2 for estimating the total degradation rate in the battery degradation analysis. The total degradation rate of four cases in Scenarios 1 and 2 are shown in Fig. 9. By integrating over the simulation period, the battery degradation of the EVs participating in the V2G process is obtained. Since parameter tuning of the battery model is not the focus of this paper, the parameters from [34] are adopted for the battery modeling. This serves solely to validate the impact of the proposed DMPC strategy on battery degradation. More accurate calculations require investigations conducted over longer time scales in V2G studies.

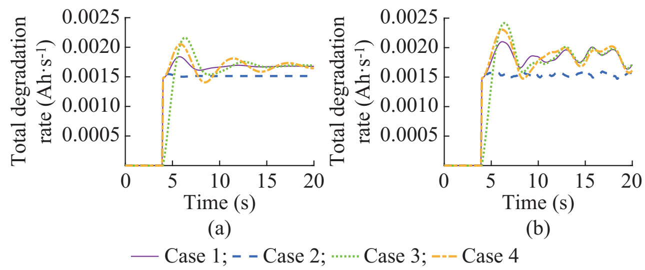

Fig. 9. Total degradation rate of four cases in Scenarios 1 and 2. (a) Scenario 1. (b) Scenario 2.

Frequent load disturbances of this nature, if solely supported by V2G responses, can cause a significant increase in charging and discharging cycles of batteries, adversely affecting their lifespan. As shown in the metrics in Supplementary Material C Table SC1, for Case 1, such V2G responses lead to an accumulated degradation rate increase of 4.5%, rising from 1.34×10^{-3} Ah to 1.40×10^{-3} Ah after time integration.

4) Computational Effort Scales with Increase of EVs

The wall-clock simulation time is measured on a desktop equipped with an Intel(R) Core(TM) i7-14700KF CPU @ 3.40 GHz. For a simulation duration of 20 s, the total computation time is 9.49 s, indicating that the optimization can be solved efficiently within each control step.

Furthermore, the computational effort of the cross-scale hierarchical framework for V2G control strategy is evaluated under different EV fleet sizes. The simulation time increases almost linearly from 9.49 s to 38.50 s as the number of EVs grows from 6 to 48. This near-linear trend indicates that the dominant computational load comes from per-EV dynamic calculations, and the model scales predictably as the fleet size increases.

By adopting the RC ECM, the proposed DMPC strategy incorporates battery state constraints and can be effectively implemented in CSs. The cross-scale DMPC embeds these constraints into the local optimization problem and quantifies the battery degradation of each EV, enabling frequency regulation with battery-aware management. The cross-scale hierarchical framework readily scales to large V2G systems and requires only the communication topology among coordinated EVs. The modeling and controller design are unified, and each EV performs local optimization with limited coordination. Moreover, the state-space formulation aligns with the sampling rates of hardware-in-the-loop (HIL) platforms, facilitating real-time implementation.

V. Conclusion

This study addresses the limitation in existing V2G FR control, where the modeling of EVs often neglects the internal battery state and degradation. A DMPC strategy based on battery state and degradation awareness is proposed to enable EVs to participate in grid frequency regulation. By embedding an RC ECM of batteries into the DMPC, the proposed DMPC strategy accurately captures the SoC and battery degradation rate, thereby enhancing the physical fidelity of the V2G model and improving its FR performance. Moreover, an equivalent degradation model of batteries is incorporated into the multi-objective optimization process, achieving coordinated management of battery states and degradation performance. Simulation results show that the proposed DMPC strategy shortens the frequency settling time by 6.5 s, reduces the V2G command tracking deviation to 2.77 kWs, improves the degradation suppression rate by more than 4.5%, and realizes more balanced power allocation among EVs. The proposed cross-scale hierarchical framework coordinates the optimization objectives between the battery and grid levels, achieving hierarchical optimization from individual batteries to the entire CS, and providing a practical pathway toward battery state and degradation-aware V2G control strategy.

Although the models facilitate theoretical validation, they have limitations in capturing the complex nonlinearities and parameter variations of real batteries, which may affect the accuracy and generalizability of the simulation results. Future research will focus on investigating time-varying parameters in the RC ECM of batteries, developing data-driven battery degradation models, extending the strategy to large-scale heterogeneous EV fleets, and conducting experimental or HIL validation to verify practical performance.

References

[1] J. Sharma, C. K. Sundarabalan, and C. Balasundar, "Advanced energy management strategy for enhancing battery lifespan in solar PV-powered EV charging stations with hybrid energy storage systems," *Renewable Energy*, vol. 251, no. 2, p. 123443, Oct. 2025.

[2] X. Xu, Z. Qiu, T. Zhang *et al*., "Distributed source-load-storage cooperative low-carbon scheduling strategy considering vehicle-to-grid aggregators," *Journal of Modern Power Systems and Clean Energy*, vol. 12, no. 2, pp. 440-453, Mar. 2024.

[3] M. A. Nasab, W. K. Al-Shibli, M. Zand *et al*., "Charging management of electric vehicles with the presence of renewable resources," *Renewable Energy Focus*, vol. 48, no. 1, p. 100536, Mar. 2024.

[4] S. Ke, L. Chen, J. Yang *et al*., "Vehicle to everything in the power grid (V2eG): a review on the participation of electric vehicles in power grid economic dispatch," *Energy Conversion and Economics*, vol. 3, no. 5, pp. 259-286, Oct. 2022.

[5] S. Ke, R. Guo, W. Mai *et al*., "Enhancing resilience of networked microgrids using V2G: a distributed model predictive control approach with non-intrusive battery surrogate," *IEEE Transactions on Industry Applications*, vol. 62, no. 2, pp. 3368-3381, Mar. 2026.

[6] K. Knezovic, S. Martinenas, P. B. Andersen *et al*., "Enhancing the role of electric vehicles in the power grid: field validation of multiple ancillary services," *IEEE Transactions on Transportation Electrification*, vol. 3, no. 1, pp. 201-209, Mar. 2017.

[7] X. Li, C. Li, F. Luo *et al*., "Electric vehicles charging dispatch and optimal bidding for frequency regulation based on intuitionistic fuzzy decision making," *IEEE Transactions on Fuzzy Systems*, vol. 31, no. 2, pp. 596-608, Feb. 2023.

[8] K. Sabahi, M. Jamil, Y. Shokri-Kalandaragh *et al*., "Deep deterministic policy gradient reinforcement learning based adaptive PID load frequency control of an AC micro-grid," *IEEE Canadian Journal of Electrical and Computer Engineering*, vol. 47, no. 1, pp. 15-21, Mar. 2024.

[9] X. Zhang, D. Shin, Y. Son *et al*., "Three-stage flexibility provision framework for radial distribution systems considering uncertainties," *IEEE Transactions on Sustainable Energy*, vol. 14, no. 2, pp. 948-961, Apr. 2023.

[10] S. Kiani, K. Sheshyekani, and H. Dagdougui, "An extended state space model for aggregation of large-scale EVs considering fast charging," *IEEE Transactions on Transportation Electrification*, vol. 9, no. 1, pp. 1238-1251, Mar. 2023.

[11] S. Gao, R. Dai, W. Cao *et al*., "Combined provision of economic dispatch and frequency regulation by aggregated EVs considering electricity market interaction," *IEEE Transactions on Transportation Electrification*, vol. 9, no. 1, pp. 1723-1735, Mar. 2023.

[12] L. Ding, S. Ke, J. Yang *et al*., "A heuristic-fuzzy improved virtual synchronous generator control strategy for charging station frequency regulation," *Journal of Energy Storage*, vol. 99, p. 113411, Oct. 2024.

[13] L. Liu, Z. Hu, and A. Mujeeb, "Automatic generation control considering uncertainties of the key parameters in the frequency response model," *IEEE Transactions on Power Systems*, vol. 37, no. 6, pp. 4605-4617, Nov. 2022.

[14] M. Wang, Y. Mu, Q. Shi *et al*., "Electric vehicle aggregator modeling and control for frequency regulation considering progressive state recovery," *IEEE Transactions on Smart Grid*, vol. 11, no. 5, pp. 4176-4189, Sept. 2020.

[15] B. Khokhar and K. P. Parmar, "A novel adaptive intelligent MPC scheme for frequency stabilization of a microgrid considering SoC control of EVs," *Applied Energy*, vol. 309, p. 118423, Mar. 2022.

[16] J. Mu, Z. Yang, D. He *et al*., "Multi-objective DMPC for heterogeneous electric vehicle platoons with communication delay under switching communication topology," *IEEE Transactions on Transportation Electrification*, vol. 12, no. 1, pp. 275-284, Feb. 2026.

[17] M. A. Nasab, M. A. Dashtaki, B. Ehsanmaleki *et al*., "LFC of smart, interconnected power system in the presence of renewable energy sources using coordinated control design of hybrid electric vehicles," *Renewable Energy Focus*, vol. 50, p. 100609, Sept. 2024.

[18] M. Khan and H. Sun, "Complete provision of MPC-based LFC by electric vehicles with inertial and droop support from DFIG-based wind farm," *IEEE Transactions on Power Delivery*, vol. 37, no. 2, pp. 716-726, Apr. 2022.

[19] S. Ke, J. Yang, L. Chen *et al*., "A frequency control strategy for EV stations based on MPC-VSG in islanded microgrids," *IEEE Transactions on Industrial Informatics*, vol. 20, no. 2, pp. 1819-1831, Feb. 2024.

[20] M. Liu, Y. Shi, and X. Liu, "Distributed MPC of aggregated heterogeneous thermostatically controlled loads in smart grid," *IEEE Transactions on Industrial Electronics*, vol. 63, no. 2, pp. 1120-1129, Feb. 2016.

[21] Y. Shi, H. D. Tuan, A. V. Savkin *et al*., "Distributed model predictive control for joint coordination of demand response and optimal power flow with renewables in smart grid," *Applied Energy*, vol. 290, p. 116701, May 2021.

[22] S. Ke, L. Ding, J. Tian *et al*., "Feedback inertia control and energy-based inertia estimation for frequency response enhancement in V2G-enabled charging stations," *Journal of Power Sources*, vol. 647, p. 237123, Aug. 2025.

[23] S. Ke, L. Ding, X. Shi *et al*., "Response characteristics and regulation feasibility of DC charging station controlled by GFM/GFL virtual inertia for grid frequency stability," *IEEE Transactions on Transportation Electrification*, vol. 11, no. 3, pp. 7743-7758, Jun. 2025.

[24] S. Ke, J. Yang, Z. Lu *et al*., "Consistency collaboration control strategy based on adaptive virtual inertia in multiple charging stations," *IEEE Transactions on Energy Conversion*, vol. 39, no. 2, pp. 896-913, Jun. 2024.

[25] S. A. G. K. Abadi, J. Choi, and A. Bidram, "A method for charging electric vehicles with battery-supercapacitor hybrid energy storage systems to improve voltage quality and battery lifetime in islanded build-

ing-level DC microgrids," *IEEE Transactions on Sustainable Energy*, vol. 14, no. 3, pp. 1895-1908, Jul. 2023.
[26] B. M. Gundogdu, S. Nejad, D. T. Gladwin *et al*., "A battery energy management strategy for U.K. enhanced frequency response and triad avoidance," *IEEE Transactions on Industrial Electronics*, vol. 65, no. 12, pp. 9509-9517, Dec. 2018.
[27] Q. Ma, W. Wei, L. Wu *et al*., "Life-aware operation of battery energy storage in frequency regulation," *IEEE Transactions on Sustainable Energy*, vol. 14, no. 3, pp. 1725-1736, Jul. 2023.
[28] X. Sun, H. Xie, D. Qiu *et al*., "Incentivizing EVs to provide frequency regulation services by aggregative game-based mechanism," *IEEE Transactions on Vehicular Technology*, vol. 73, no. 9, pp. 12787-12800, Sept. 2024.
[29] S. Stock, J. Hagemeister, S. Grabmann *et al*., "Cell teardown and characterization of an automotive prismatic LFP battery," *Electrochimica Acta*, vol. 471, p. 143341, Dec. 2023.
[30] J. Gong, D. Wasylowski, J. Figgener *et al*., "Quantifying the impact of V2X operation on electric vehicle battery degradation: an experimental evaluation," *eTransportation*, vol. 20, p. 100316, May 2024.
[31] C. Mu, W. Liu, and W. Xu, "Hierarchically adaptive frequency control for an EV-integrated smart grid with renewable energy," *IEEE Transactions on Industrial Informatics*, vol. 14, no. 9, pp. 4254-4263, Sept. 2018.
[32] Z. Afshar, H. Rahmanei, I. Bhogaraju *et al*., "Hierarchical frequency and SOC control of power grids with battery energy storage systems," *IEEE Transactions on Power Electronics*, vol. 39, no. 7, pp. 7925-7937, Jul. 2024.
[33] R. Arya, S. Modi, and S. Ganguli, "Parameter estimation of first-order RC model of lithium-ion batteries in electric vehicles using slime mould algorithm," in *Linear and Nonlinear System Modeling*. Hoboken: Wiley-Scrivener, 2024, pp. 173-195.
[34] M. Petit, E. Prada, and V. Sauvant-Moynot, "Development of an empirical aging model for li-ion batteries and application to assess the impact of vehicle-to-grid strategies on battery lifetime," *Applied Energy*, vol. 172, pp. 398-407, Jun. 2016.

Song Ke received the Ph.D. degree in electrical engineering from Wuhan University, Wuhan, China, in 2024. He is currently a Postdoctoral Fellow with The Hong Kong Polytechnic University, Hong Kong, China. His research interests include user behavior modeling, battery management system, and intelligent control strategy design in vehicle to grid.

Weijie Mai received the B.Eng. degree in electrical engineering from The University of New South Wales, Sydney, Australia, in 2012, and the Ph.D. degree in electrical engineering from The Hong Kong Polytechnic University, Hong Kong, China, in 2017. He currently serves as the Vice-President at Shenzhen Auto Electric Power Plant Co., Ltd., Shenzhen, China. His research interests include electric vehicle charging, energy storage system, smart grid, demand side management, demand response optimization, power system stability and control, planning and operation, and computational intelligence application.

Jinpeng Tian received the Ph.D. degree in mechanical engineering and electrical engineering from Beijing Institute of Technology, Beijing, China, and Swinburne University of Technology, Melbourne, Australia, in 2021 and 2022, respectively. From 2023 to 2024, he worked as a Postdoctoral Research Fellow at the Hong Kong Polytechnic University, Hong Kong, China, where he is currently a Research Assistant Professor. His research interest includes management of energy storage system, particularly rechargeable battery.

Ruohan Guo received the Ph.D. degree in electrical engineering from the Swinburne University of Technology, Melbourne, Australia, in 2024. He is currently a Postdoctoral Research Fellow with the Department of Electrical and Electronic Engineering and the Research Centre for Grid Modernisation at the Hong Kong Polytechnic University, Hong Kong, China. His research interests include battery health prognostics and management, fault detection, and screening and repurposing of retired battery for second-life application.

Shangyang He received the M.S. degree in automation from the Huazhong University of Science and Technology, Wuhan, China, in 2023. He is working toward the Ph.D. degree in the Department of Electrical and Electronic Engineering at Hong Kong Polytechnic University, Hong Kong, China. His research interests include operation of ultra-fast electric vehicle charging station, energy storage system, deep learning, deep reinforcement learning, and graph neural network.

Chi Yung Chung received the Ph.D. degree in electrical engineering from The Hong Kong Polytechnic University, Hong Kong, China, in 1999. He is currently the Head of the Department of Electrical and Electronic Engineering, the Chair Professor of Power Systems Engineering, and the Founder and Director of the Research Centre for Grid Modernisation at the Hong Kong Polytechnic University. His research interests include smart grid, renewable energy, power system stability and control, planning and operation, computational intelligence application, electricity market, energy storage, and electric vehicle charging.